Microstructure and Properties of Aluminum Alloy 2090 Weldments

Weld properties are correlated to the effects that EBW and GTAW have on microstructure formation

BY A. J. SUNWOO AND J. W. MORRIS, Jr.

ABSTRACT. The effects of welding on aluminum alloy 2090 are examined along with the metallurgical changes associated with welding and aging. The results of the study show that the gas tungsten arc (GTA) and electron beam (EB) weldment properties are controlled by the precipitate size and distribution. There is a tradeoff between strength and elongation. In the as-welded condition, solid solution strengthening is the primary strengthening mechanism present. As a result, the weldment strengths are less than 200 MPa (29 ksi), but the elongations are greater than 4%. In the postweld aged condition, an inhomogeneous distribution of solutes results in an inhomogeneous distribution of precipitates, causing strain localization. Although the weldment strengths increase, the weldment elongations decrease precipitously. The peak strengths of EB and GTA weldments are obtained aging at 160°C (320°F) for 32 h with 75% joint efficiency and at 190°C (374°F) for 16 h with 65% joint efficiency, respectively. Aging at 230°C (446°F) leads to coarsening of precipitates as well as the intermetallic constituents; the weldment strengths deteriorate rapidly, but the elongations improve. The best overall weldment properties are obtained in the solution heat treated and aged conditions, and are associated with a homogeneous distribution of strengthening precipitates.

Introduction

A material's properties are determined by its composition and microstructure. In turn, microstructure is determined by composition and processing. For aluminum alloy (AA) 2090-T8E41, the right blend of chemical composition and thermal-mechanical processing produced a microstructure, that, combined with its composition, resulted in properties that are equivalent or superior to current commercially available high-strength aluminum alloys at room and cryogenic temperatures, respectively (Refs. 1–5). AA 2090, with a combination of high specific strength and toughness, and high specific modulus, is a promising material for the weight-limited cryogenic structures. However, for some cryogenic applications, welding is required.

The weld properties are determined by the same factors as the base metal properties: microstructure and composition. During welding, a localized region of the base metal is melted and resolidified. The fusion zone morphology, as well as the solute distribution, depend on the constitutional undercooling of the individual process. Hence, different welding processes affect the weld properties differently. The objective of this research is to examine the effects of welding processes, with overall composition held constant, on the microstructure and solute segregation, and to correlate its effects to the weldment properties. In addition, the weldment aging responses are also examined.

Experimental Procedure

The chemical composition of as-received 2090 in wt-% is 3.0Cu-2.2Li-0.12Zr-Al. The as-received 2090 sheet was in the T3 temper (solution heat treated and stretched 4.6%). The sheet was cut into weld coupons of 102 × 203 mm (4 × 8 in.). The weld coupons were machined from their initial thickness of 4.3 mm (0.17 in.) to approximately 3.2 mm (0.12 in.) in order to remove distortion and processing oxide. Prior to welding, the weld coupons were chemically cleaned using 5 vol-% sodium hydroxide in water, followed by concentrated nitric acid.

KEY WORDS

2090 Al-Cu-Li Alloy
Weldability/Aging
Electron Beam Weld
Gas Tungsten Arc Weld
Aging Temperature
Joint Efficiency
Hot Cracking
Grain Size Effects
Solution Heat Treat
Fractography

The two welding processes chosen for this study were gas tungsten arc (GTA) and electron beam (EB) welding. These processes were used to produce a significant difference in the as-solidified microstructure and solute segregation. The welding parameters for GTAW and EBW are listed in Table 1. Autogenous, bead-on-plate welds were produced transverse to the rolling direction. For GTA welding, direct current electrode negative (DCEN) (straight polarity) was used, and welding was conducted on a water-cooled chill block in an argon atmosphere. These precautions, mechanical and chemical cleaning, welding in an inert atmosphere, and use of a water-cooled chill block, were taken to prevent porosity and hot cracking.

The base metal of T3 temper and as-welded weldments were aged at 160°, 190°, and 230°C, to the peak-aged condition. In addition to the postweld aged conditions, the solution-heat-treated-and-aged (SHTA) conditions of the base metal and both EB and GTA weldments were also investigated. The optimum temperatures for SHT were determined using differential scanning calorimetry. The SHTA process consists of a three-step heat treatment: 535°C (995°F) for 15 min, 550°C (1022°F) for 15 min, water quench, and subsequent aging at 160°C. Figure 1 shows the tensile specimen configurations. The overall specimen size was 89 mm (3.5 in.) with

A. J. SUNWOO and J. W. MORRIS, Jr., are with the Center for Advanced Materials Lawrence Berkeley Laboratory and the Department of Materials Science and Engineering, University of California, Berkeley, Calif.

Based on paper presented at the 69th Annual AWS Meeting, held April 17–22, 1988, in New Orleans, La.

Table 1—Welding Parameters

	GTAW	EBW
Current	110 A	9.5 mA
Voltage	18–20 V	80 kV
Travel speed	6.4 mm/s	16.9 mm/s
Electrode diameter	2.4 mm	–
Electrode angle	90–120 deg	–
Electrode-to-work distance	1.6 mm	280 mm
Shielding gas	75% He-25% Ar	
Vacuum pressure		2×10^{-4} Torr

25.4 mm (1 in.) gauge length.

Transmission electron microscope (TEM) specimens were prepared by mechanically polishing the disks to 0.125-mm thickness (0.005 in.) and jet-electropolishing using 75 vol-% methanol and 25 vol-% nitric acid solution at −30°C (−22°F). The foils were viewed at 100 kV using a Phillips 301 microscope.

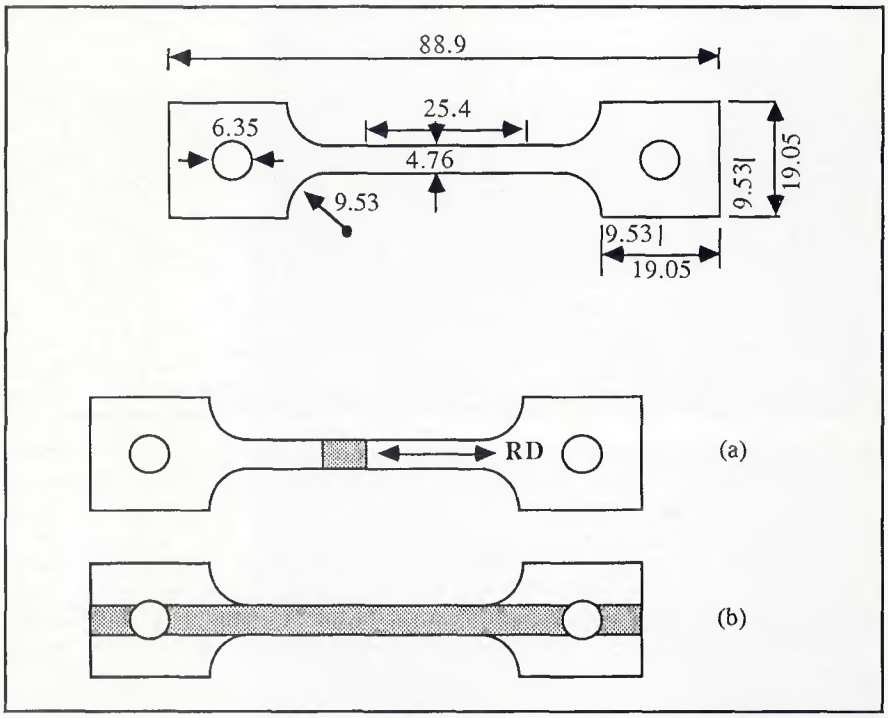

Fig. 1—Tensile specimen configuration. A—Composite specimen; B—all-weld-metal specimen. Dimensions are in mm, and the shaded regions represent the fusion zone

Results

Chemical and Energy Dispersive X-Ray Analysis

The results of atomic absorption spectroscopy indicated that the composition of autogenous GTA welds was similar to that of the base metal, 2.8Cu-2.2Li-0.12Zr-Al. There was no Li loss; instead, a slight Cu loss was found, which may be attributable to scatter in the data.

Although the change in overall weld composition was insignificant, differences in dendrite morphology and in degree of solute segregation were expected between the EB and GTA fusion zones. EB welding, with high energy density and low heat input (and consequently a fast cooling rate) produces a fine equiaxed dendrite structure with limited solute segregation. The observed EB weld dendrites were equiaxed, and their average size was approximately 10 μm. The GTA welding, on the other hand, is distinctly different from the EB welding. Gas tungsten arc welding is characterized by low energy density and high heat input, and consequently, a slower cooling rate that produces a cellular dendrite structure with more pronounced solute segregation. The average cellular dendrite size of the GTA fusion zone was approximately 20 μm. The dendrite size was determined by averaging both length and width of the dendrites.

In order to qualitatively determine the solute segregation, energy dispersive x-ray (EDX) line scans were conducted across the dendrites of as-welded EB and GTA fusion zones. Figure 2 shows the concentration profiles of Al and Cu in the EB fusion zone. Different sensitivity scales were used for Al and Cu due to the large difference in concentrations. The Cu scale was an order of magnitude larger than the Al scale. The Al concentration profile showed Al-depleted regions near the dendrite boundaries and at intermetallic phases. The Cu concentration profile of the same line showed peaks near the boundaries but not in the intermetallic phases. Overall, these changes in Al and Cu concentrations were small in the EB fusion zone.

With GTA welding, more pronounced solute segregation was expected than in EB welding. For the GTA fusion zone, Zr was also analyzed, since Al-depleted regions were present at the intermetallic phases without the corresponding Cu peaks. Figure 3A shows the concentration profiles of Al and Cu using the same sensitivity scales as in Fig. 2. The Al valleys and Cu peaks were better defined in the GTA fusion zone, but the general trend of the profiles was similar to the EB fusion zone, with Al valleys corresponding to Cu peaks at the dendrite boundaries. Figure 3B shows the concentration profiles of Al and Zr within the same region. The Al concentration profile is the same as in Fig. 3A. The Zr concentration profile showed small fluctuations along the den-

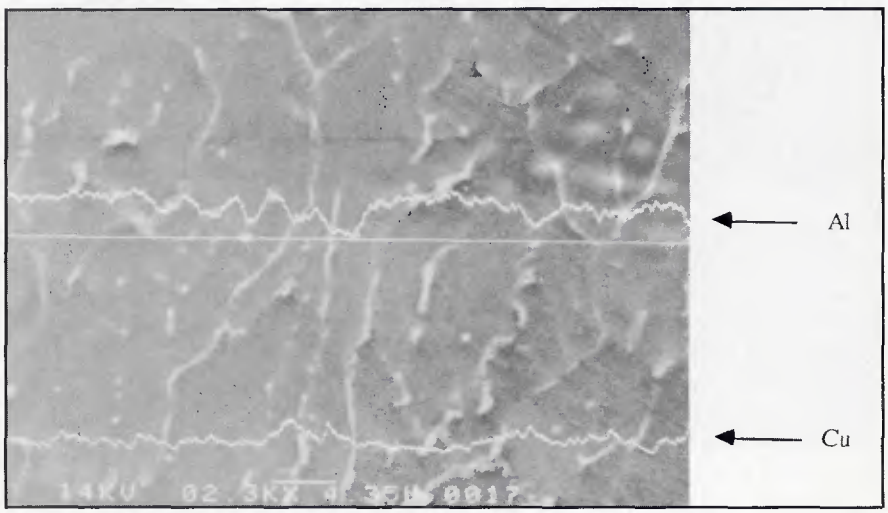

Fig. 2—EDX line scan of Al and Cu in the EB fusion zone

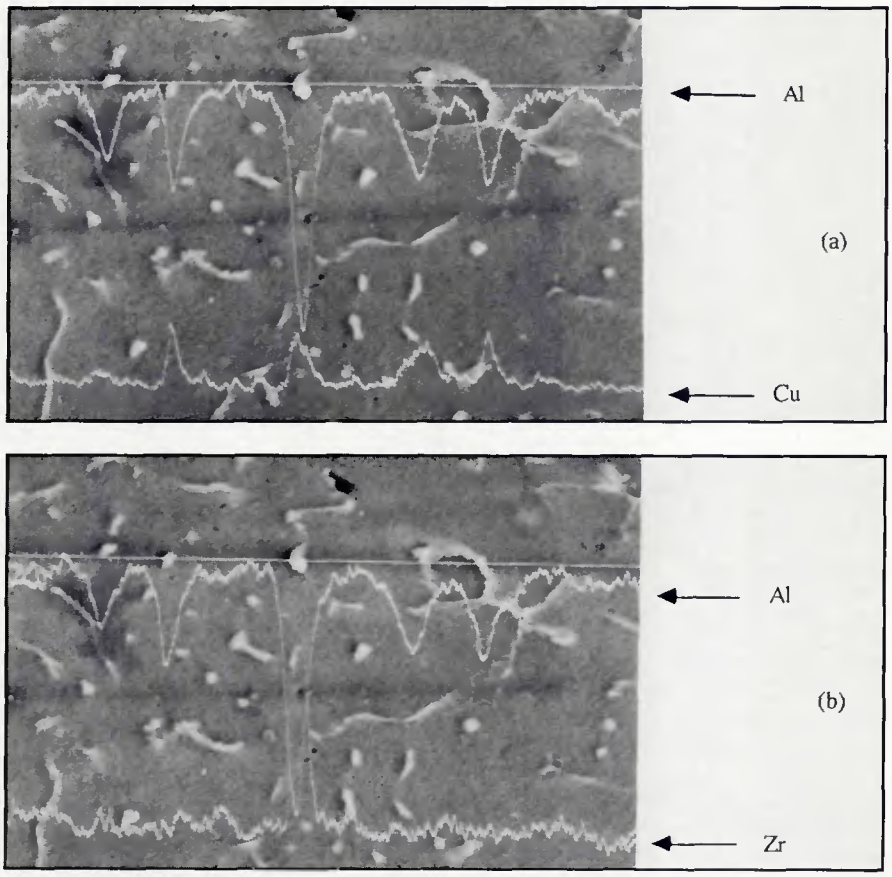

Fig. 3—EDX line scan of the GTA fusion zone. A—Concentration profiles of Al and Cu; B—concentration profiles of Al and Zr

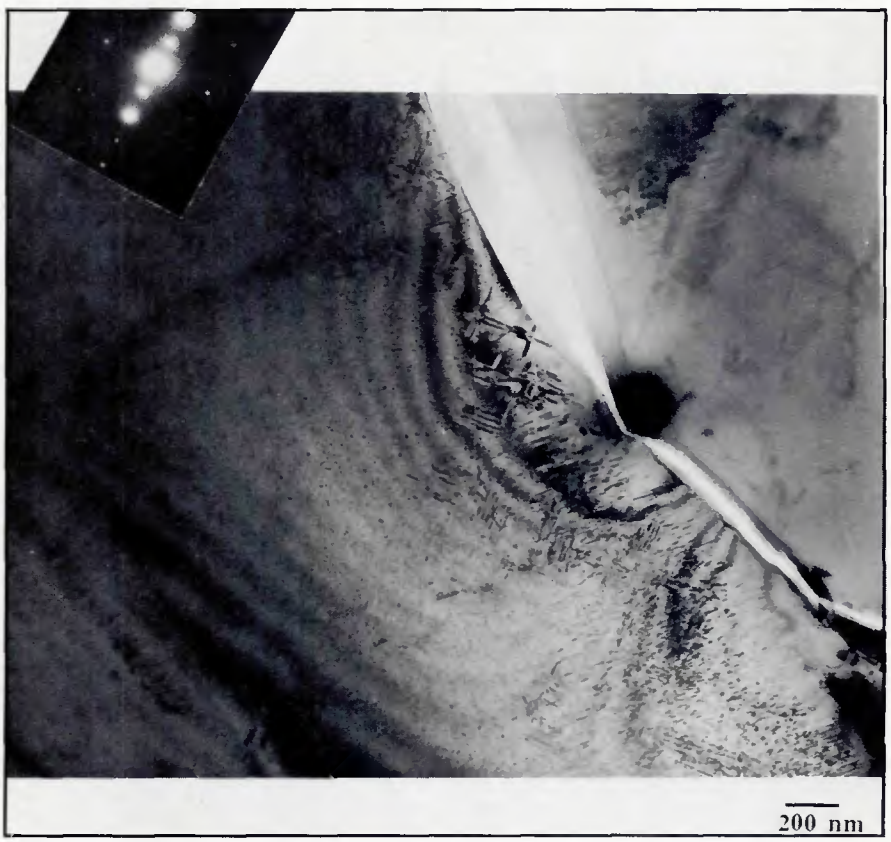

Fig. 4—TEM bright field image of a peak-aged GTA fusion zone; near [100] orientation

drite, matching Al-depleted regions. The line scan indicated the presence of a Zr-containing phase at the dendrite boundary. These distinct differences in the EBW and GTAW fusion zones affected the aging response and, in turn, the weldment properties.

TEM Analysis

The AA 2090 obtains its strength through a homogeneous distribution of strengthening precipitates (Refs. 3–5). The major strengthening precipitates are $\delta'(Al_3Li)$, $T_1(AL_2CuLi)$, and $\theta'(Al_2Cu)$. The δ' is a spherical metastable phase that precipitates within the grain. The θ' is a plate-like phase that also precipitates within the grain. The T_1 is a plate-like, equilibrium phase that precipitates at dislocations and grain boundaries. The $\beta'(Al_3Zr)$ is a dispersoid particle used as a grain refiner that precipitates during the ingot thermal treatment. Among the phases that adversely affect the properties are $\delta(AlLi)$, $T_2(Al_6CuLi_2)$, and Al_7Cu_4Fe (Ref. 6–8). The δ and T_2 are the equilibrium phases and are known to precipitate only at the grain boundaries.

For this research, the distribution of the plate-like precipitate phases is more important than their individual nature, so they will be merely described as plate-like precipitates. To characterize precipitate morphology and its distribution in the fusion zone, TEM was done on the as-welded, peak-aged, and SHTA GTAW fusion zones. For the EB welds, the fusion zone was not wide enough to make good TEM specimens.

In the as-welded condition, the precipitation was minimal; β' and δ' phases were present, but no plate-like precipitates were found. In the postweld aged condition, the solute gradients lead to precipitate gradients within the dendrite. Figure 4 shows a bright field image of a peak-aged specimen in the near [100] orientation. The SAD pattern showed distinct superlattice diffraction spots with streaks in the [001] direction. The micrograph revealed a fine distribution of δ' phase and an inhomogeneous distribution of plate-like precipitates around the boundary. A large spherical intermetallic phase, possibly δ or T_2 phase, was also found at the boundary. In the SHTA condition, SHT provided a homogeneous distribution of solutes and subsequent aging provided a homogeneous distribution of precipitates. Figure 5 shows a bright field image of a SHTA specimen in the near [211] orientation. Again, the SAD pattern showed distinct superlattice diffraction spots. The micrograph revealed a homogeneous distribution of both plate-like precipitates and δ' precipitates. The distribution and morphology of these precipitates control the strength and elongation of the weldments.

Mechanical Properties

The yield strengths, ultimate tensile strengths (UTS), and elongations of base metals, EB weldments, and GTA weldments are presented in Table 2. The results of the aging study indicated that 2090 strength degraded after exposure to temperatures greater than 200°C. The best overall strength and elongation combination for the base metal followed aging at 160°C for 32 h. The base metal peak-aged at 190°C for 16 h showed an insignificant improvement in strength, but had higher elongation. However, specimens aged at 230°C for 4 and 16 h were severely overaged; the yield strengths of the specimens aged for 16 h decreased to less than 50% of the 160°C peak-aged condition, and elongation had lowest value of all aging conditions.

For EB weldments, the highest strengths were obtained by aging at 160°C for approximately 32 h. The aging response of the EB weldments was similar to that of the base metal when aged at 190°C and at 230°C. As the aging temperature increased, the peak strength was achieved in a shorter time, as expected. However, the peak yield strength at 160°C was higher than that of 190°C. The EB weldments also became overaged at 230°C.

Higher yield strength was achieved for GTA weldments aged at 190°C than at 160°C. The peak yield strength at 190°C was reached between 16 and 24 h, while the yield strength of weldments aged at 160°C continued to increase and peaked beyond 32 h. Aging at 230°C also adversely affected GTA weldment properties. The joint efficiencies of EB and GTA weldments in the near peak-aged condition were 75% and 65%, respectively.

Fig. 5—TEM bright field image of a solution heat treated and aged GTA fusion zone; near [211] orientation

As the weldment strength increased with aging, the weldment elongation decreased precipitously—Table 2. In the as-welded condition the weldment elongations were greater than 4%. In the peak-aged condition, the elongations were less than 1%. Visual observation of the tested as-welded EBW and GTAW specimens revealed localized deformation in the fusion zone and minimal deformation in other areas. In the tested peak-aged weldments, there was no evidence of deformation in the fusion zone. In the overaged condition, the weldment elongation improved slightly. It is noteworthy

Table 2—Tensile Test Results

Heat Treatment (°C/h)	EBW/GTAW/BM 0.2% Yield Strength (MPa)	EBW/GTAW/BM UTS[a] (MPa)	EBW/GTAW/BM Total Elongation (%)
T3; As-welded	195/175/281	288/270/352	4.4/4.4/9.3
PWA[b]			
160/8	359/253/517	407[a]/326[a]/592	0.6/1.2/8.9
160/16	—/295/560	—/314[a]/605	—/0.8/9.4
160/32	438/314/574	445[a]/372[a]/608	0.3/0.8/9.4
190/2	—/—/—	401[a]/—/—	0.1/—/—
190/4	357/291/493	380[a]/350[a]/538	0.5/0.7/8.8
190/16	350/334/496	363[a]/371[a]/547	0.3/0.5/11.2
190/24	—/325/—	—/363[a]/—	—/0.5/—
230/2	—/230/—	—/288/—	—/1.2/—
230/4	314/259/338	354[a]/320[a]/416	0.7/1.0/11.0
230/16	274/248/279	321[a]300[a]/371	1.3/1.2/7.8
SHT A[c]			
160/4	311/315/313	415[a]/396[a]/403[a]	5.4/2.5/6.9
160/16	416/384/413	479[a]/435[a]/485[a]	1.8/1.1/10.1
All weld metal[d]			
As-welded	—/137/—	—/250/—	—/17.0/—
160/32	—/254/—	—/322/—	—/1.5/—

(a) Fracture strength.
(b) PWA = postweld aged.
(c) SHT&A = solution heat treated and aged after welding.
(d) See Fig. 1B.

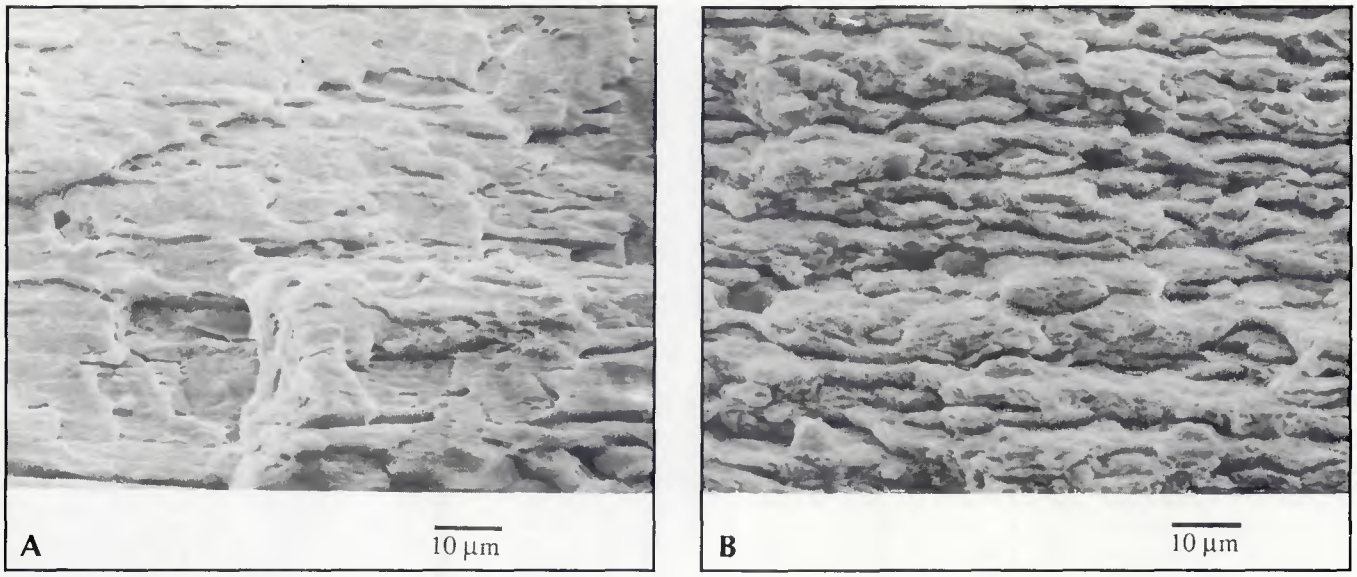

Fig. 6—SEM fractographs of base metal. A—Aged at 160°C for 16 h; B—aged at 230°C for 16 h

that although the composite specimens showed only 4% elongation, the all-weld-metal GTA specimens showed 17% elongation. Similar to the composite specimens, the all-weld-metal elongation decreased to 1.5% in the near peak-aged condition.

After the base metal and welded imens were postweld solution heat treated and aged at 160°C for 4 h, the yield strengths of the base metal and weldments were equivalent, and both weldment elongations increased, especially the EB weldments. At 16 h, the yield strengths of the EB weldment and base metal continued to be equivalent, but the EB weldment elongation decreased by a factor of 3 from 5.4 to 1.8%. Aging from 4 to 16 h, the strengths of GTA weldments increased by approximately 25% from 285 to 355 MPa (41.3 to 51.9 ksi), but the elongation decreased by 40% from 2.5 to 1.1%.

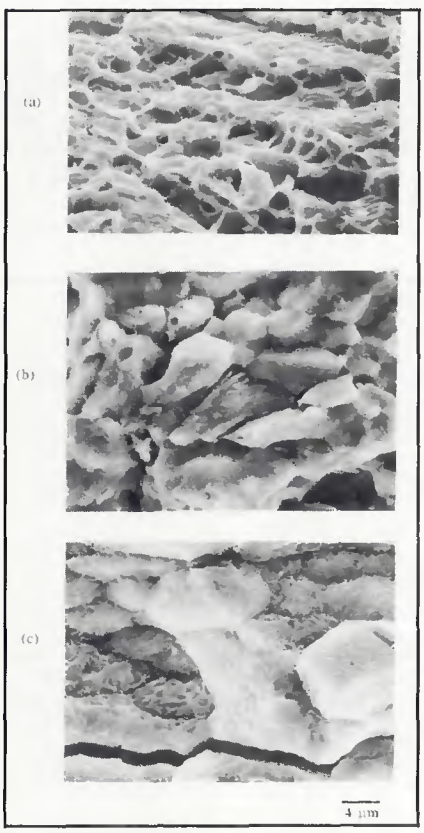

Fig. 7—SEM fractographs of EB weldments A—As-welded condition; B—aged at 160°C for 32 h; C—solution heat treated and aged at 160°C for 16 h

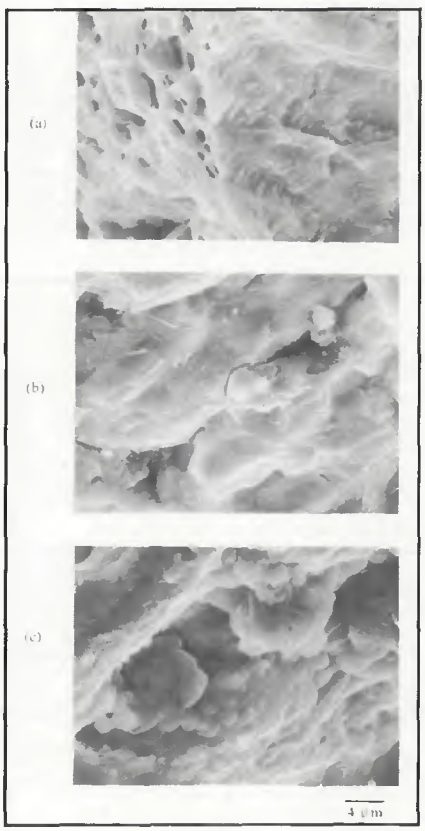

Fig. 8—SEM fractographs of GTA weldments. A—As-welded condition; B—aged at 190°C for 16 h; C—aged at 230°C for 16 h

Fractography

Scanning electron microscope (SEM) fractographs showed different fracture modes for the base material, EB weldments and GTA weldments. The base metal fractured in shear. Figure 6 shows the SEM fractographs of the base metal in peak-aged and overaged conditions. In the peak-aged condition, the fracture surface appeared planar-transgranular, whereas in the overaged condition, the surface appeared ductile with subgrain delamination.

The fracture mode and failure location in the EB weldments changed with aging condition. Figure 7 shows EB fracture surfaces in the as-welded, peak-aged and SHTA conditions. The fracture surface of as-welded EB specimens revealed ductile fracture with void formation and slip evident—Fig. 7A. Failures occurred at the fusion boundary. In the peak-aged condition, the fracture surface revealed interdendritic fracture (Fig. 7B) and failures occurred within the fusion zone. Very fine spherical particles were observed at the boundaries. For the SHTA condition, uniform void formation occurred at the dendrite surfaces, but the fracture mode continued to be interdendritic—Fig. 7C. In the overaged condition, small spherical particles coarsened to become globular particles at the dendrite boundaries (similar to Fig. 8C). This also promoted interdendritic fracture.

The fracture modes of the GTA weldments were ductile dimple with second-

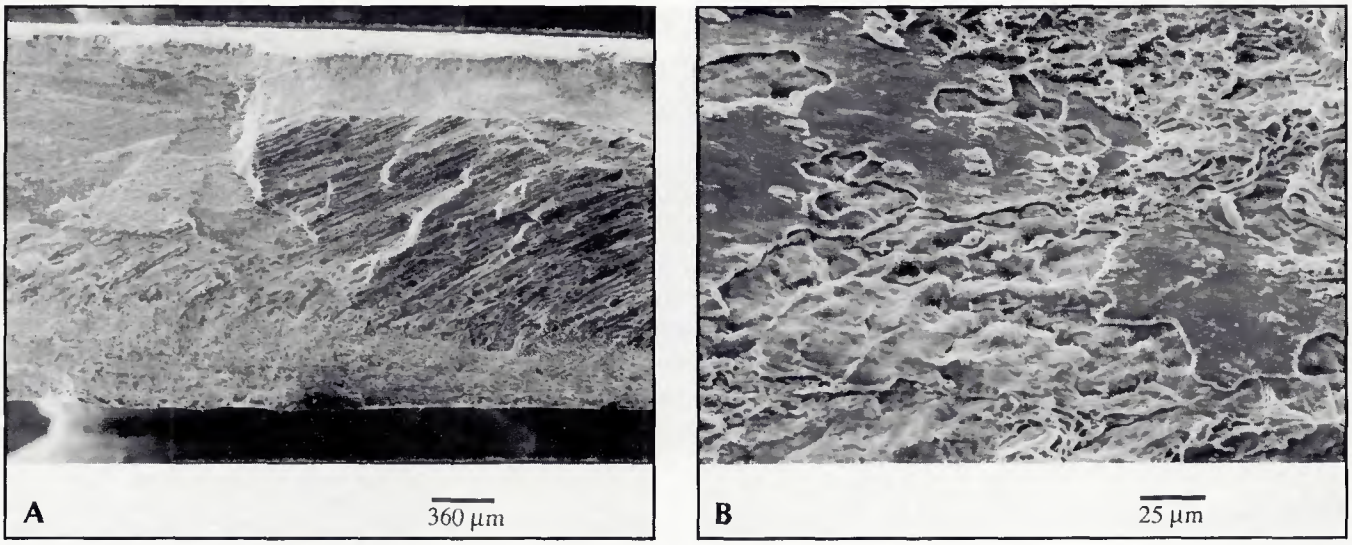

Fig. 9 — SEM fractographs of GTA weldment in solution heat treated and aged at 160°C for 4 h. A — Overall fracture surface; B — partially melted region

ary cracks at the dendrite boundaries. Failure occurred close to the center of the fusion zone. Figure 8 shows the SEM fractographs of the as-welded, peak-aged, and overaged conditions. The as-welded GTA fracture surface was similar to the as-welded EB fracture surface with void formation and slip evident along the dendrite boundaries — Fig. 8A. In the peak-aged condition, spherical intermetallic phases decorated the dendrite boundaries, and in the overaged condition, these phases became globular, as shown in Figs. 8B and 8C. Figure 9 shows the GTA specimen fracture surface after SHTA for 4 h. There were three distinct regions: the lamellar microstructure of base metal, the dendritic microstructure of the weld, and the partially melted region (PMR) of the HAZ — Fig. 9A. Figure 9B shows the PMR, identified by its smooth surface decorated with various size particles. The PMR was also present on the other fracture surfaces of SHTA GTA weldments. Fracture may have initiated at the PMR regions, resulting in a premature failure.

Discussion

Effect of Grain Size

The grain size is known to influence the strength of an alloy. However, for the range of grain sizes considered, the influence of grain size on strength is found to be small. In general, the grain size dependence on the strength can be predicted using the Hall-Petch relationship (Ref. 9). The average grain size of the GTA fusion zone is 150 μm, while the average grain size of the base metal in the longitudinal direction is an order of magnitude larger. Assuming that the SHT produced a homogeneous distribution of solutes in the GTA weldments and erased prior thermal mechanical processing (TMP) of the base metal, the effect of grain size on strength is compared for the SHTA conditions — Table 2. Qualitatively, the GTA weldment is expected to be stronger. However, equivalent yield strengths are found for the GTA weldments and the base metal aged at 160°C for 4 h. With a continuous aging, the yield strength of the GTA weldments is approximately 30 MPa (4.3 ksi) lower than that of base metal. This indicates that there are other metallurgical factors contributing to the properties. Thus, the grain size has a limited influence on the strength of the alloy.

Effect of Solute and Precipitate Strengthening

The differences in base metal properties and weldment properties can be explained by their solute/precipitate distribution. For the base metal, TMP is utilized to attain a homogeneous distribution of solutes and to control the formation and distribution of the strengthening phases during aging. By influencing precipitation behavior, a combination of high strength and toughness is obtained. The major strengthening phases in 2090 are the plate-like T_1 and θ' precipitates.

Prior TMP effects are almost erased in the fusion zone of the weldments. Instead, the degree of solute segregation is established during welding. The EBW fusion zone shows more limited solute segregation than that of the GTAW fusion zone. This distinct difference between the EB and GTA fusion zones affects the solid solution strengthening and aging response and, in turn, the weldment properties.

In the as-welded condition, there is a limited strengthening precipitate in the fusion zone, and hence, the primary strengthening mechanism is solid solution strengthening. When the effects of solid solution strengthening on the yield strengths of as-welded EB and GTA weldments are compared, the difference in yield strengths is only 20 MPa. When the near peak-aged yield strengths of EB and GTA weldments are compared, the difference in strengths is at least 100 MPa (14.5 ksi). Similarly, when yield strengths of the GTA weldments postweld aged at 160°C for 16 h and SHTA aged at 160°C for 16 h are compared, the yield strength of the SHTA weldments is 90 MPa (13 ksi) higher. These comparisons indicate that the precipitate strengthening mechanism is a more effective strengthening mechanism than solid solution strengthening in the fusion zone. Also, a homogeneous distribution of solutes, which leads to a more homogeneous distribution of precipitates, is important for the aged properties.

The weldment strength and elongation are inversely related and are closely tied to the tensile failure mode. Since solid solution strengthening is the only strengthening mechanism of significance present in the as-welded condition, dislocation motion is less effectively impeded than if strengthening precipitates are present. As a result, the weldment elongation is greater than 4%, and the failure mode is ductile fracture. In the postweld aged condition, due to inhomogeneous distribution of the precipitates, strain is localized near the dendrite boundaries and subsequently leads to interdendritic failure (Refs. 10, 11). As the weldment becomes overaged, the precipitates as well as the intermetallic phases are coarsened (Ref. 12, 13). The distribution of the precipitates becomes nonuniform within the dendrite, and the primary strengthening mechanism becomes less effective. Thus, the dislocation movement be-

comes easier and the elongation improves slightly. By homogenizing the solute/precipitate distribution, both strength and elongation are improved. In the SHT and underaged condition, the precipitate size has not been optimized and hence, the dislocation movement is not as effectively impeded, leading to lower strength and higher elongation. However, at longer aging times, a precipitate-free zone has formed adjacent to the dendrite boundary intermetallic phases, especially in the EB fusion zones. Since PFZ is softer than other areas, a localized strain develops and causes interdendritic ductile fracture (Ref. 10, 12).

Conclusions

The effects of welding on AA 2090 were studied along with the metallurgical changes associated with welding and aging. The weldment properties are controlled by the precipitate size and distribution. There is a tradeoff between strength and elongation. The following specific conclusions are drawn.

1) In the as-welded condition, solid solution strengthening is the primary strengthening mechanism present. As a result, the weldment strengths are less than 200 MPa, but the elongations are greater than 4%.

2) In the postwelded aged condition, an inhomogeneous distribution of solutes results in an inhomogeneous distribution of precipitates, causing strain localization. Although the weldment strengths increase, the weldment elongations decrease precipitously.

3) The highest peak yield strengths of EB and GTA weldments are obtained at 160°C for 32 h with 75% joint efficiency and at 190°C for 16 h with 65% joint efficiency, respectively. Aging at 230°C leads to coarsening of precipitates, as well as the intermetallic constituents. As a result, weldment strengths deteriorate rapidly and elongations improve.

4) The best overall weldment properties are obtained in the solution heat treated and aged conditions, due to a homogeneous distribution of strengthening precipitates.

Acknowledgments

The authors would like to thank the Aluminum Company of America for providing the material and B. Olsen of the Lawrence Livermore National Laboratory for producing the EB welds. This work is supported by the Director, Office of Energy Research, Office of Fusion Energy, Development and Technology Division of the U.S. Department of Energy under contract #DE-AC03-76SF00098.

References

1. Glazer, J., Verzasconi, S. L., Dalder, E. N. C., Yu, W., Emigh, R. A., Ritchie, R. O., and Morris, J. W. 1986. *Adv. Cryo. Eng.* 32:397-404.

2. Glazer, J., Verzasconi, S. L., Sawtell, R. R., and Morris, J. W. 1986. *Metall. Trans.,* 18A: 1695 to 1701.

3. Rioja, R. J., Bretz, P. E., Sawtell, R. R., Hunt, W. H., and Ludwiczak, E. A., 1983. *Aluminum Alloys II.* Conf. Proc., eds. E. A. Starke, Jr., and T. H. Sanders, Jr., pp. 1781-1797. The Metallurrgical Society of AIME.

4. Staley, J. T., Rioja, R. J., Wyss, R. K., and Liu, J. 1987. Alcoa ALTC Division Report, 04-87-JD-34-56.

5. Ashton, R. F., Thompson, D. S., Starke, Jr., E. A., and Lin, F. S. 1986. *Aluminum-Lithium Alloys III.* Conf. Proc., eds. C. Baker, P. J. Gregson, S. J. Harris, and C. J. Peel, pp. 66-77. The Institute of Metals. London, England.

6. Tosten, M. H., Vasudevan, A. K., and Howell, P. R. 1986. *Aluminium-Lithium Alloys III.* Conf. Proc. eds. C. Baker, P. J. Gregson, S. J. Harris, and C. J. Peel, pp. 490-495. The Institute of Metals. London, England.

7. Rioja, R. J., and Ludwiczak, E. A. 1985. *Aluminum-Lithium Alloys III,* Conf. Proc., eds. C. Baker, P. J. Gregson, S. J. Harris, and C. J. Peel, pp. 471-482. The Institute of Metals. London, England.

8. Toston, M. H., Vasudevan, A. K., and Howell, P. R. 1986. *Aluminum-Lithium Alloys III.* Conf. Proc., eds. C. Baker, P. J. Gregson, S. J. Harris, and C. J. Peel, pp. 483-489. The Institute of Metals. London, England.

9. Dollar, M, and Thompson, A. W. 1987. *Acta. Metall.* 35 (1):227-235.

10. Vasudevan, A. K., and Doherty, R. D. 1987. *Acta Metall.* 35 (6):1193-1219.

11. Gräf, M., and Hornbogen, E. 1977. *Acta Metall.* 25:883-889.

12. Thomas, G., and Nutting, J. 1959. *Journal of Institute of Metall.* 88:81-90.

13. Nicholson, R. B., Thomas, G., and Nutting, J. 1958. *Journal of Institute of Metals.* 87:429-438.